


Article

Anchor Design of a Ring Joint Based on Reliability in a Precast Shear Wall Structure

Jian Zhou ^{1,2} , Xudong Zhi ^{1,2,*}, Feng Fan ^{1,2}, Anliang Jiao ³ and Hongliang Qian ^{1,2}¹ Key Lab of Structures Dynamic Behaviour and Control of the Ministry of Education, Harbin Institute of Technology, Harbin 150090, China² Key Lab of Smart Prevention and Mitigation of Civil Engineering Disasters of the Ministry of Industry and Information Technology, Harbin Institute of Technology, Harbin 150090, China³ China Construction Seventh Engineering Division Corp. Ltd., Zhengzhou 450004, China

* Correspondence: zhixudong@hit.edu.cn

Received: 6 June 2019; Accepted: 12 August 2019; Published: 15 August 2019



Abstract: Precast buildings have been widely used owing to its outstanding features. As these buildings consist of a combination of various components, the mechanical properties of the connections play a critical role in the overall performance of the structure, particularly the vertical connections in shear wall members. A new connection called ring joint is proposed for precast buildings, and test pieces were designed to analyze the anchor performance. The damage phenomena and test data were observed and recorded. The displacement, force, and strain were analyzed, and the results indicated that the anchor length was a key factor and the connection was safe and reliable under reasonable design. Numerical analysis was conducted to explore the mechanical mechanism, and a bearing capacity model was proposed combining the bond and dowel effects simultaneously. Anchor length was determined based on reliability analysis under various conditions, and other suggestions were proposed. All these could guarantee the mechanical properties of the connection, as well as safety and reliability, and promote the popularization and application.

Keywords: precast structure; ring joint; numerical analysis; bearing capacity model; reliability analysis

1. Introduction

The industrialisation of buildings is the future direction for the development of the construction industry, and this transformation will allow for sustainable development of the construction industry. Prefabricated shear wall structure systems are widely used in high-rise buildings, which can reduce resource consumption and facilitate environmental protection. In prefabricated buildings, the connections are critical for the mechanical performance of the structure in meizoseismal areas [1], particularly the vertical connection of the components, the quality and reliability of the connection are crucial to the architecture.

Various precast building connection methods have been proposed by scholars, and their tensile properties have been evaluated, including grouted sleeve connections, etc. [2–4]. The grouted sleeve has been developed [5,6], and its uniaxial tensile properties have been extensively studied [7–10]. Research has shown that the bearing capacity is affected by the grouted sleeve strength, grout strength, rebar diameter, and bond strength [11]. The bond strength of the grout and rebar plays a key role in determining the bearing capacity, and has thus attracted the attention of researchers. In addition, a novel grouted rolling pipe splice has been proposed and its mechanical performance has been tested [12,13]. A plug-in filling hole for lap-joint steel bars, was tested considering the rebar diameter, anchor length, and concrete strength, and the results indicated that the connection was reliable [14]. In design theory, the anchoring test was carried out and the calculation formula of the lap length

design was given based on the reliability analysis [15], including straight reinforcement and mechanical anchoring. Liu [16] carried out the pull-out test on grouted-filled lap splice, and established the formula for calculating the ultimate overlap length, and carried out reliability analysis based on the central point method. Both had given the anchor length with reliability guarantee. In the above connections, the complicated joining processes and expensive connecting equipment greatly increases the cost, and the research also indicated that the connection had anchor failure due to the poor interval quality of the connection. Therefore, the concealed operation of the above connection method has a certain degree of security risks in application.

A new connection called ring joint comprising interlocked ring rebar and inserted horizontal rebar has been proposed. The connection area is poured on-site, and a continuous beam is then formed, which strengthens the joining area significantly, as shown in Figure 1a. This connection saves the sleeve consumption, and there are no concealed operations, which can guarantee the quality and reliability under reasonable design conditions. In research, Lu [17] conducted cyclic tests considering the height–width ratio and the joining height with the connecting area in the middle of the walls, and the results indicated that the connection was safe. To evaluate the mechanical performance, cyclic in-plane tests [18] and the flexural out-of-plane tests [19] were conducted when the connection was applied to the bottom of the shear wall. The above experimental research indicates that the joint can meet the relevant specifications in China. There is still a lack of research on mechanical mechanism and application of anchor design, so further research is necessary.

In this paper, the pull-out test was carried out to evaluate the anchoring performance. The mechanism was clear and the bearing capacity model could predict the bearing capacity well. Anchor length was determined based on reliability analysis and design suggestions were proposed, which could promote the application of the connection technology.

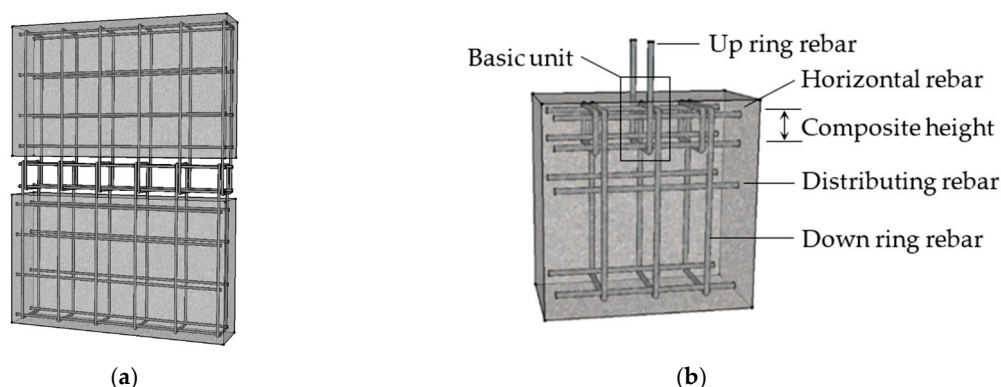


Figure 1. Schematic diagram of the ring joint connection. (a) Connection diagram; (b) Specimen schematic.

2. Experimental Research

Pull-out test was carried out to evaluate the bearing capacity, and composite height and relative horizontal position were taken into consideration. Ring rebar pull-out and fracture were observed, and data was analyzed. The connection could work well under reasonable design.

2.1. Model Design and Properties Test

Each specimen consists of three basic units and its dimension is $400 \times 200 \times 400$ mm considering the characteristics of the joint, and a schematic diagram in Figure 1b is used to show interval details. Composite height is the overlap size of the up and down rebars, and four levels is taken into consideration, as shown in Table 1, and each group consists of three specimens. Horizontal position is the relative horizontal position of the up and down rebars in one basic unit, and it consists of adjacent and interval arrangement. The specification of rebars is HRB400. The concrete specification in all groups is C30.

Table 1. List of specimens.

Group	Composite Height CH/mm	Horizontal Position HP	Horizontal Rebar ϕ /mm	Horizontal Rebar ϕ /mm
A1	60	Adjacent [Figure 1b]	8	10
A2	80	Adjacent	8	10
A3	100	Adjacent	8	10
A4	160	Adjacent	8	10
B1	100	Interval [Figure 5a]	8	10

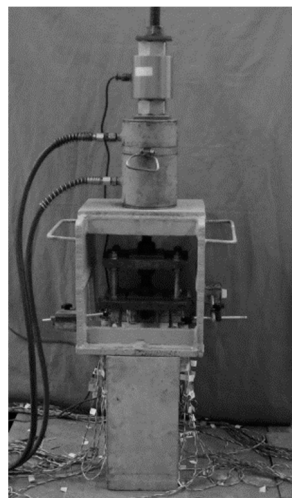
The mechanical properties of the rebar were obtained, and the results are summarised in Table 2. Concrete test pieces with dimensions of 150 mm \times 150 mm \times 150 mm were prepared during pouring and subjected to the same maintenance conditions. The concrete cube compressive strength and elastic modulus are 37.04 MPa and 3.19×10^4 N/mm², respectively.

Table 2. Mechanical properties of steel rebar.

Diameter (mm)	f_y (MPa)	f_u (MPa)	ϵ_y ($\mu\epsilon$)
8	435.6	661.6	2178
10	436.5	668.7	2237

2.2. Test and Measuring Device

The test setup and measurement is illustrated in Figures 2 and 3. To achieve synchronous loading, a steel plate was welded to the rebar at a distance of 100 mm from the test piece. A reaction frame device was designed for counter force loading. The test piece, reaction frame, hydraulic jack, and force sensor were connected by steel rods. A preloading of 5 kN was implemented to detect the loading and collecting devices. In the official loading, the loading was slowly increased until the specimen had broken and the test was stopped when the ring rebar fractured or the bearing capacity decreased to 85% of the peak load. Two sensors were arranged on both sides of the specimen to measure the displacement of the rebars, and the strain values were recorded by gauges (Figure 3) arranged for mechanical analysis and numerical model validation. The force, displacement, and strain were all recorded simultaneously.

**Figure 2.** Test and measuring setup.

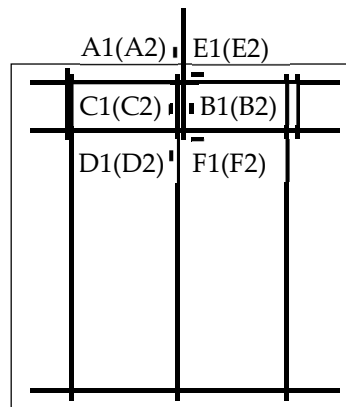


Figure 3. Strain gauges.

2.3. Results Analysis

2.3.1. Phenomena and Modes

Two failure modes were observed including ring rebar pull-out and ring rebar fracture, the former mode occurred in group A1 and the latter mode occurred in other groups. In this section, A11 and A31 are chosen as being representative to show the details in loading.

Specimen A11 was in the elastic stage until 40 kN, then some cracks appeared around the up-ring rebars, and some cross cracks were observed on the surface of the concrete. Some V-shaped cracks appeared on both sides when loaded to 43 kN. After that, the cracks developed rapidly and reached 5 mm, and the up-ring rebar and horizontal rebars yielded at 46 kN and 50 kN respectively. When loaded to 70 kN, more vertical run-through cracks appeared at the down-ring rebar position. The up-ring rebar was pull-out at a load of 81 kN, and concrete spalling and inverted V-shaped deformation of horizontal rebars were observed. The crack and failure mode are shown in Figure 4a. Specimen A31 was initially in the elastic phase, as was A11. Up-ring rebar yielded when loaded to 46 kN, some cracks appeared around the rebars and gradually developed into oblique cracks at 52 kN. V-shaped cracks appeared on both sides when loaded to 58 kN, and cracks increased with loading. The horizontal rebar yielded at 63 kN, and horizontal cracks appeared at the down-ring rebar position when loaded to 65 kN. Up-ring rebar yielded when loaded to 80 kN, 92 kN was recorded as the ultimate load when one side of rebar fractured, while the horizontal rebars were always in the flexible phase. The final failure mode are shown in Figure 4b.



Figure 4. Cracks and failure patterns of specimens. (a) The crack and failure mode of A11; (b) The crack and failure mode of A31.

The interval arrangement was shown in Figure 5a, and the damage process was basically the same as the specimens in group A3 and ring rebar fracture occurred. A number of vertical cracks appeared at the down-ring rebar position and horizontal cracks appeared at the down horizontal rebars in final

failure mode. Obviously, this arrangement is an unfavorable factor. The crack and failure mode are shown in Figure 5.

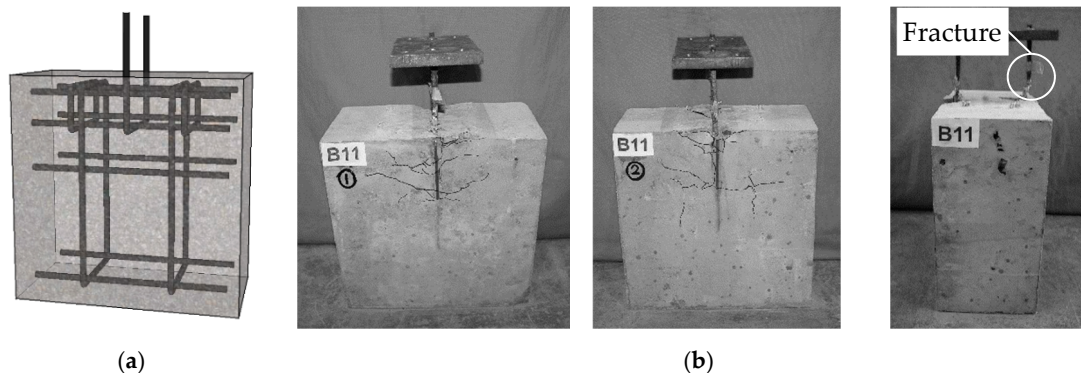


Figure 5. Crack and failure mode of interval arrangement in Group B. (a) Interval arrangement; (b) Crack pattern of B11.

2.3.2. Bearing Capacity and Deformation Performance

The force *versus* displacement curves were the basis for evaluating the bearing capacity performance, and the results were shown in Figure 6. The curves are initially linear and specimens are in flexible phase. The gradient of the curves decreases and specimens enter the elastoplastic stage with increasing loading. The curves decrease abruptly in the pull-out specimens, and the curves show an increasing trend before the plastic stage in rebar fracture specimens. The curves develop without abrupt changes until the rebar fractures. Obviously, small discrepancies in curves indicates that the bearing performance is stable and reliable. The yield ratio (F_y/F_u) and ductility coefficient (Δ_u/Δ_y) are important indicators to evaluate the bearing capacity and deformation capacity of the joint.

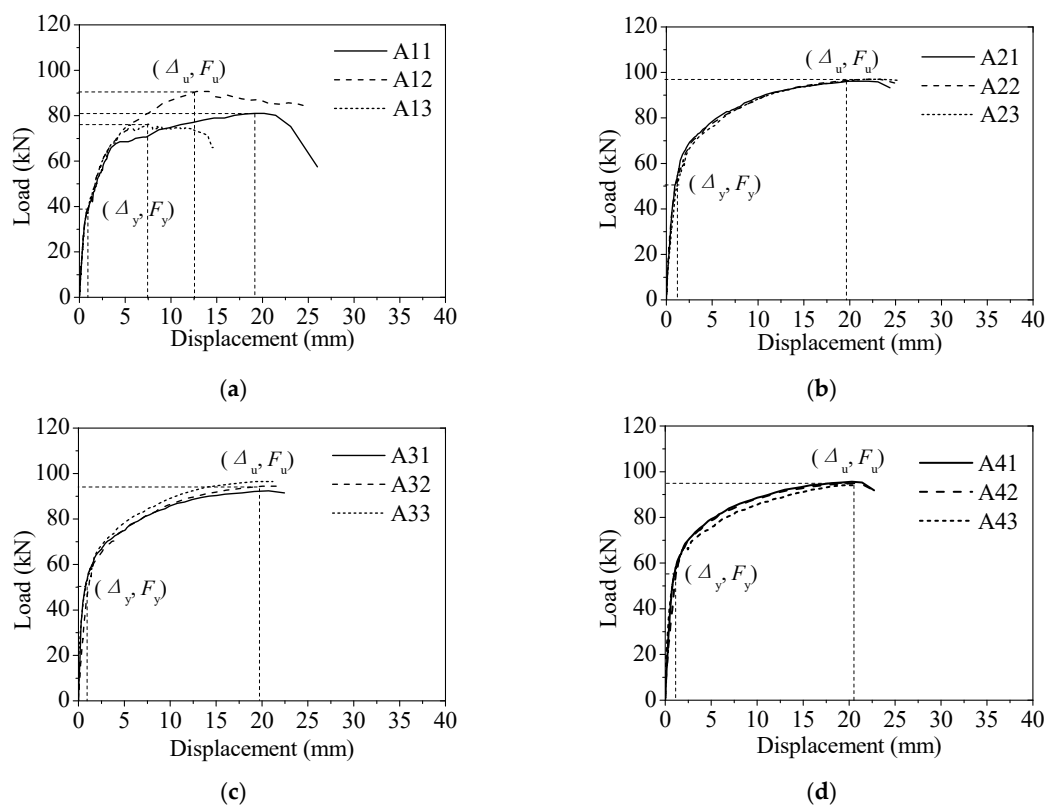


Figure 6. Cont.

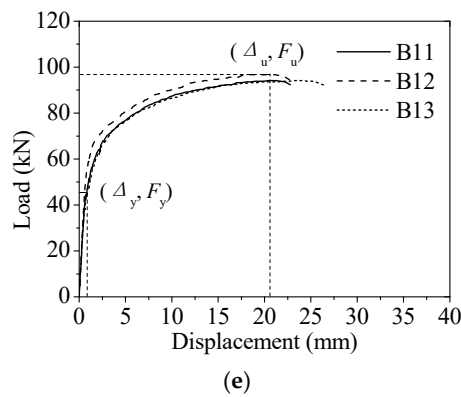


Figure 6. Load-displacement curves of specimens. (a) Group A1; (b) Group A2; (c) Group A3; (d) Group A4; (e) Group B1.

In terms of composite height, four levels were used to evaluate the effects on the bearing performance. The yield load increases from 4% to 31% with a single-step increase (Figure 7a), and the yield ratio increases 6%–16% per stage (Figure 7b). The ductility coefficient increases 1%–20% per stage, as can be seen in Figure 7c. In addition, the cracks were significantly reduced with increasing composite height. Therefore, increasing the composite height could significantly improve the anchoring performance of the concrete to ring rebars, thereby improving the bearing performance.

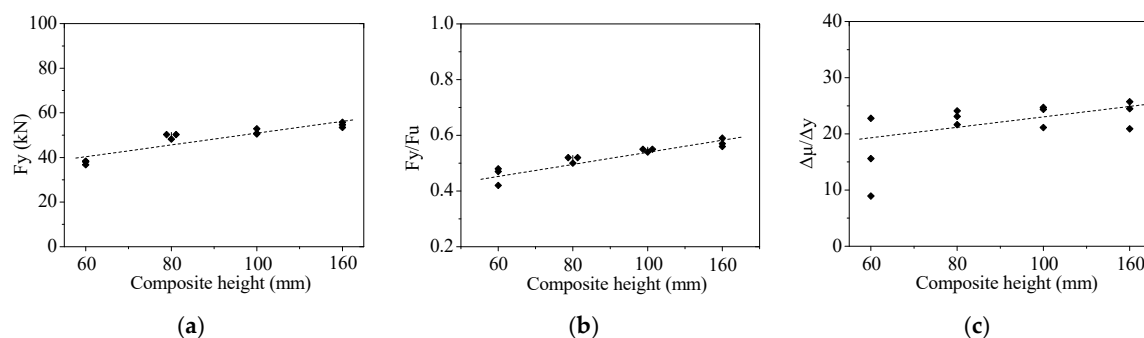


Figure 7. Results analysis of composite height tests. (a) Yield strength analysis; (b) Yield ratio analysis; (c) Ductility analysis.

Compared with the benchmark group A3, the interval arrangement in group B (Figure 5a) exhibits an 11% decrease in the yield load, and it also results in an 11% decrease in the yield ratio and a 53% increase in the ductility factor. Therefore, the interval arrangement not only decreases the bearing capacity, but also undergoes a greater deformation, that is an unfavorable factor.

3. Model Verification

Numerical analysis was conducted to explore the mechanical mechanism and provide the basic data for bearing capacity model, considering the nonlinearity of materials and geometries; the number of connection units was taken into consideration.

3.1. Numerical Model

A numerical analysis was conducted using the commercial program ABAQUS. A suitable model has the ability to not only accurately simulate the stress process, but also improve the analysis efficiency. To model the concrete and rebar, 8-node reduced integral solid elements (C3D8R) and 2-node linear beam elements were used, respectively. Considering the complexity of the rebar and the dowel effect of the horizontal rebar, a beam element model was selected for the rebar. A bond-slip contact relationship will significantly increase the analytical workload, and can easily cause corner unit distortion without

convergence. In addition, the mechanical mechanism of the rebar is the focus of this study. Therefore, the ideal co-node embedded model was adopted for the contact between the rebar and concrete [20]; the boundary condition was consistent with the tests. Considering the efficiency and precision, a grid size of 20 mm was adopted for the concrete. To improve the analysis accuracy for the rebar, the grid size was 10 mm. The numerical model is shown in Figure 8.

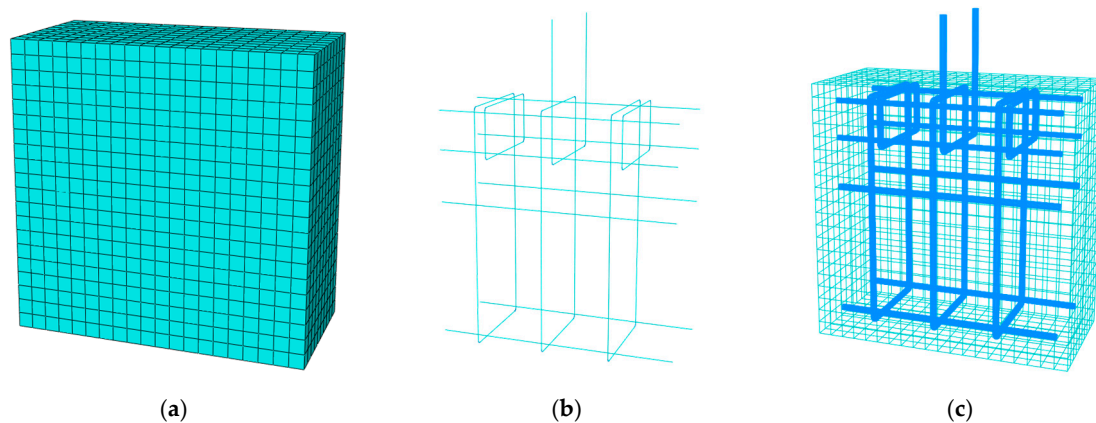


Figure 8. The numerical model. (a) Concrete elements; (b) Steel elements; (c) Perspective of whole model.

The nonlinearity of the materials and geometry was taken into consideration. The elastoplastic damage constitutive relation could better reflect its nonlinear behaviour. The Concrete Damaged Plasticity material was used for the concrete [21], while the steel material model was implemented using the user material subroutine [22]. The standard calculation in static analysis was applied, and the load was cumulatively applied at loading intervals of 1 kN until failure of the test piece.

3.2. Strain Analysis

To validate the numerical model, the load applied to the rebars was distributed based on the proportion of strain A in the test, and the experimental data was compared to the numerical analysis results. The inner and lower parts were analyzed comprehensively, and the strain-load curves at positions B and D were compared, as shown in Figure 9. The curves show that the numerical model results are in good agreement with the experimental results, and thus the model can be applied for mechanism analysis as well as further research.

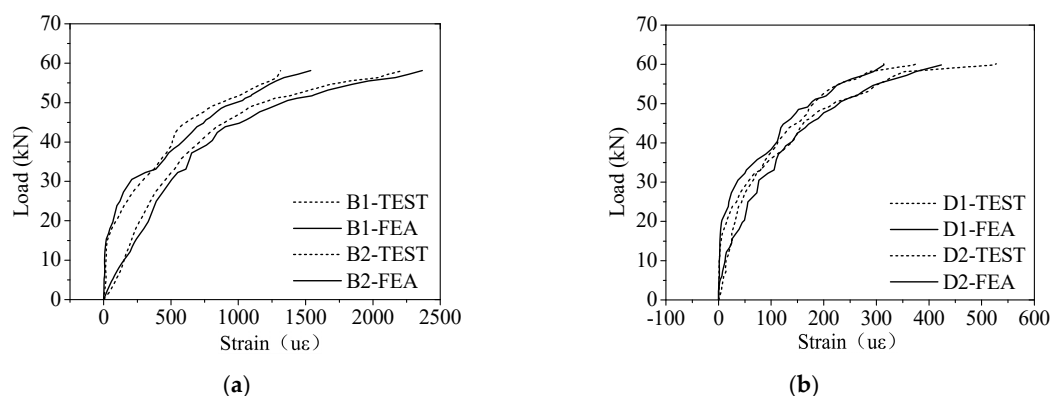


Figure 9. Verification of the numerical results for the strain values. (a) Strain curves at B1 and B2; (b) Strain curves at D1 and D2.

For further evaluation, a greater yield strength was only defined for the up-ring rebar. The load was 67.24 kN when the down horizontal rebar yielded (Figure 10a); the test value was 63.04 kN, and

thus the numerical results were 6.66% greater than the test results. A partial diagram is shown in Figure 10b, and the stress distribution is presented in Figure 10c, which reflects the dowel action; a deformation is observed consistent with the experimental observations. Thus, the model not only reflects the internal mechanical behaviour, but also reflects the combination of the anchoring and dowel effects. Therefore, it can be used for further research.

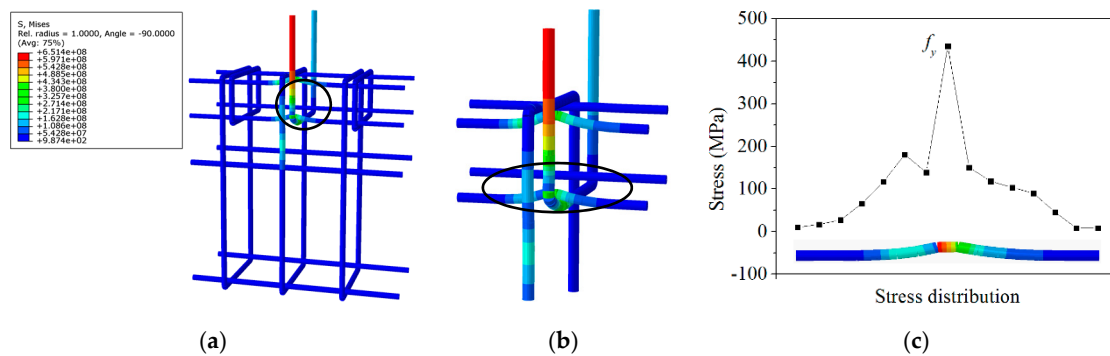


Figure 10. Stress analysis of the down horizontal rebar in the specimen. (a) Yielding of the horizontal rebar; (b) Partial display; (c) Stress distribution.

3.3. Effect of the Number of Connection Units on the Results

Models composed of 3, 5, 7, and 9 units were established to analyze the effect on the results, and the result for the intermediate unit in each specimen was reported. The strain values at positions C, E, F, and D when the up-ring rebar yielded are illustrated in Figure 11. The strain curves for positions C and D were almost unaffected, while the strain curves at positions E and G decreased as the number of ring units increased, until gradually stabilising after the model consisted of at least five units. Considering the accuracy and efficiency, the model with five units is selected.

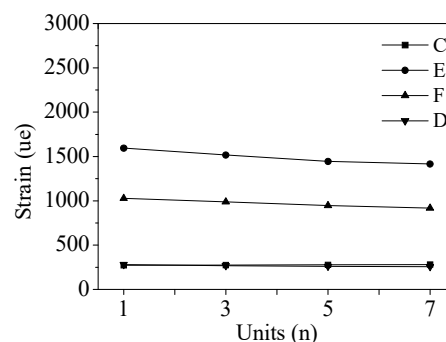


Figure 11. Effect of the number of ring units on the strain results.

4. Bearing Capacity Model

Obviously, the rebar fracture is an ideal failure mode. The experimental and numerical results served to reveal the mechanical mechanism and the bearing capacity consisted of the anchoring effect of the ring rebar and the dowel action of the horizontal rebar. A bearing capacity model was proposed and could predict bearing capacity well.

4.1. Basic Bearing Capacity Model

Drawing on existing research, a ring rebar can be symmetrically separated, and the bearing capacity could be calculated according to the calculation method for bent rebar. The schematic diagram for the bent rebar is shown in Figure 12. The bond stress, τ_u , can be calculated with Equation (1), and the bearing capacity can then be calculated [15].

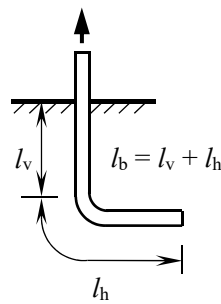


Figure 12. Schematic of bent rebar.

$$\tau_u = \left[\left(0.82 + 0.9 \frac{d}{l_v} \right) \left(1.6 + 0.7 \frac{c}{d} \right) + 12.5 \frac{d}{l_v} \sqrt{\frac{l_h}{l_v}} \right] f_t \quad (1)$$

Equation (1) is a stiffness equation expressed in the form of strength, where the first term represents the bonding effect of the straight anchor segment, l_v , and the second term represents the effect of the rear anchor segment, l_h , on the bonding performance of the straight anchor segment. When $l_h \geq 7d$, the displacement–load curves continues to rise after the bending point and anchoring is safe and reliable.

The ability of the horizontal rebar to bear the shear force is called the dowel action. At the splicing interface of the prefabricated structure, the horizontal rebar serves to resist and transfer the axial load of the ring rebar, and the dowel action is the only transmission mechanism for the shear force [23,24]. Research has shown that the crack pattern of the horizontal rebar is mainly manifested by the combined failure modes of the generated shear forces and tensile forces. Accurately predicting the bearing capacity is of great significance for ensuring the safety of the joints. Li and Rasmussen [25,26] investigated the role of the horizontal rebar and proposed a mathematical model considering the effect of damage that could accurately predict the bearing capacity. The model is applied under the condition of no splicing interface, as shown in Equations (2)–(5); the mechanical diagram was shown in Figure 13.

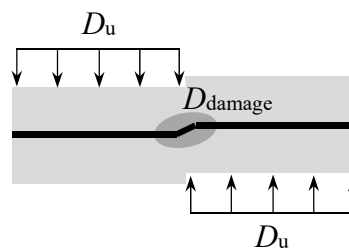


Figure 13. Mechanical diagram of dowel action.

$$D_u = 1.3 d_h^2 (f_c \cdot f_y)^{\frac{1}{2}} \quad (2)$$

$$D_{\text{damage}} = 3 \times 10^{-6} X^2 + 0.0212X \quad (3)$$

$$X = d_h^2 (f_c \cdot f_y)^{\frac{1}{2}} \quad (4)$$

$$D_c = D_u - D_{\text{damage}} \quad (5)$$

In the bearing capacity model, D_u was the basic calculation model, and D_{damage} was the attenuation of bearing capacity of the horizontal rebar caused by local comprehensive damage of concrete. X was the material factor. Finally, D_c , the modified model was obtained.

4.2. Parametric Study

Five factors were considered for the parametric analysis based on the models of the anchoring and dowel actions, as listed in Table 3. Rebar fracture was observed in all models, and the load, f_{y-R} , was recorded when the ring rebar yielded and the horizontal rebar was still in the elastic phase. In bearing capacity analysis, only the yield strength of the ring rebar was increased to yield the horizontal rebar, and the corresponding load, f_{y-HR} , was recorded. The ratio of f_{y-HR}/f_{y-R} was used to evaluate the capacity reserve and results are summarised in Table 4.

Table 3. List of factors in the bearing capacity analysis.

No.	Factor	Symbol	Unit	Parametric Level			
1	Rebar diameter	d_r	mm	8	10	12	14
2	Concrete grade	C	MPa	C25	C30	C35	C40
3	Composite height	CH	mm	75	100	125	150
4	Width of ring unit	W_r	mm	125	150	175	200
5	Horizontal rebar diameter	d_h	mm	8	10	12	14

Table 4. Bearing capacity analysis and model analysis.

No.	Model List				Reserve Analysis			Bearing Capacity Analysis				
	d_r	C	CH	W_r	d_h	f_{y-R}	f_{y-HR}	$\frac{f_{y-HR}}{f_{y-R}}$	F_u	D_c	P	$\frac{P}{f_{y-HR}}$
L1	8	C30	100	150	10	36.17	70.58	95.13	-	-	-	-
L2	10	C30	100	150	10	56.52	76.75	35.79	70.04	15.64	77.08	0.43
L3	12	C30	100	150	10	81.69	86.94	6.43	-	-	-	-
L4	14	C30	100	150	10	110.78	95.00	14.24	-	-	-	-
M1	10	C25	100	150	10	56.52	74.79	32.32	60.70	14.29	67.14	-10.23
L2	10	C30	100	150	10	56.52	76.75	35.79	70.04	15.64	77.08	0.43
M3	10	C35	100	150	10	56.52	82.39	45.77	77.05	16.87	84.64	2.73
M4	10	C40	100	150	10	56.52	85.22	50.78	84.05	17.79	92.06	8.02
N1	10	C30	75	150	10	56.52	75.56	33.69	-	-	-	-
L2	10	C30	100	150	10	56.52	76.75	35.79	70.04	15.64	77.08	0.43
N3	10	C30	125	150	10	56.52	88.53	56.63	83.14	15.64	90.18	1.86
N4	10	C30	150	150	10	56.52	98.59	74.43	96.70	15.64	103.74	5.22
O1	10	C30	100	125	10	56.52	70.93	25.50	72.82	15.64	79.86	12.58
L2	10	C30	100	150	10	56.52	76.75	35.79	70.04	15.64	77.08	0.43
O3	10	C30	100	175	10	56.52	82.59	46.13	68.93	15.64	75.97	-8.02
O4	10	C30	100	200	10	56.52	86.12	52.37	68.84	15.64	75.88	-11.89
P1	10	C30	100	150	8	56.52	73.47	29.99	-	-	-	-
L2	10	C30	100	150	10	56.52	76.75	35.79	70.04	15.64	77.08	0.43
P3	10	C30	100	150	12	56.52	86.71	53.41	-	-	-	-
P4	10	C30	100	150	14	56.52	95.77	69.44	-	-	-	-
Q1	8	C30	100	150	8	33.17	69.89	110.70	56.83	10.56	61.58	-11.89
L2	10	C30	100	150	10	56.52	76.75	35.79	70.04	15.64	77.08	0.43
Q3	12	C30	100	150	12	70.65	93.23	31.96	87.38	22.59	97.54	4.63
Q4	14	C30	100	150	14	96.56	120.47	24.76	107.07	30.71	120.89	0.35

Note: The units of $\left(\frac{f_{y-HR}}{f_{y-R}}\right)$ and $\left(\frac{P}{f_{y-HR}}\right)$ are %; models marked with “-” were not used.

In group L1–L4, the horizontal rebar diameter is 10 mm, and the reserve decreases from 95.13% to -14.24%, at which there is no reserve, as the diameter of the up-ring rebar increases from 8 mm to 14 mm. In group P1–P4, the diameter of the up-ring rebar is 10 mm, and the reserve increases from 29.99% to 69.44% as the diameter of the horizontal rebar increases from 8 mm to 14 mm. In group Q1–Q4, the up-ring rebar is consistent with the horizontal rebar, and the reserve decreases from 110.70% to 24.76% as the diameter increases from 8 mm to 14 mm, demonstrating a high safety reserve. Research has shown that the reserve is low or zero when the diameter of the ring rebar is larger than

that of the horizontal rebar. However, the reserve is improved when the diameter of the ring rebar is larger or equal to that of the horizontal rebar. The diameter thus plays a critical role in the bearing capacity, and it is recommended that the diameter of the ring rebar should be consistent with that of the horizontal rebar considering the bearing capacity reserve and economic factors. As the concrete grade increases from C25 to C40 in group M1–M4, the reserve increases from 32.32% to 50.78%. The reserve increases from 16.85% to 74.43% as the composite height increases from 75 mm to 150 mm in group N1–N4. As the width of the ring rebar increases from 125 mm to 200 mm in group O1–O4, the reserve increases from 25.50% to 52.37%. Therefore, the connection is safe and reliable with an improved reserve under a reasonable design.

Based on the parametric analysis and bearing capacity reserve analysis, some suggestions are proposed: the diameter of the horizontal rebar should be consistent with that of the ring rebar; at least two rows of the horizontal rebar should be arranged at the corner of the closed area; the composite height and the width of the ring rebar should be at least 100 mm and 125 mm, respectively. The concrete grade should be better than C25, and the concrete grade of the connection area should be one level higher than that of the components.

In-depth analysis were conducted based on models that satisfy the above suggested conditions, and the bearing capacity analysis results are summarised in Table 4. A bearing capacity model was proposed through linear fitting by considering the anchoring and dowel actions comprehensively, as given in Figure 14 and Equation (6).

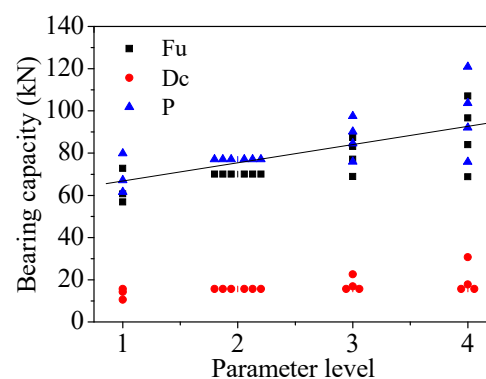


Figure 14. Linear curve of bearing capacity model.

$$P = F_u + 0.45D_c \quad (6)$$

By substituting Equations (2)–(5) into (6) and ignoring the small effect of other factors, the bearing capacity model is obtained, as shown in Equation (7).

$$P = 2\pi d(l_v + l_h)\tau_u + 0.58d^2(f_c \cdot f_y)^{\frac{1}{2}} \quad (7)$$

5. Reliability-Based Anchoring Design

Anchoring limit state equilibrium equation is shown in this paper. On the basis, according to the relevant statistical parameters and the determined reliability indexes of anchoring length and stiffness, the anchorage length of the ring rebar is obtained under various conditions.

5.1. Equilibrium Equation for the Limit State

Anchor failure or rebar fracture may occur when the up-ring rebar is under tension. Under the maximum tension, the minimum anchoring length at which the up-ring rebar reaches the yield strength without anchor failure is called the critical anchor length. The up-ring rebar reaches the yield strength,

and anchorage damage occurs simultaneously, which is called the limit state, i.e., the anchoring force is equal to the yield load of the up-ring rebar. The anchorage limit state is shown in Figure 15.

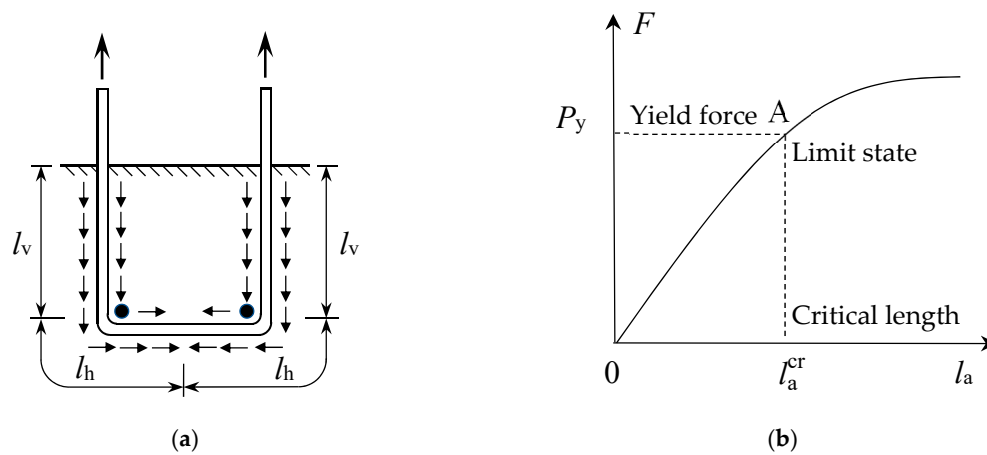


Figure 15. Anchorage limit state. (a) Mechanical diagram of the ring rebar; (b) Anchoring curve.

In the limit state, the ultimate bearing capacity is P , i.e., the anchorage resistance, R , of the rebar can be expressed as Equation (8).

$$R = P = 2\pi d(l_v + l_h)\tau_u + 0.58d^2\sqrt{f_c \cdot f_y} \quad (8)$$

The ultimate pull-out force of the up-ring rebar is F_u , i.e., the effect, S , caused by the up-ring rebar is expressed as Equation (9).

$$S = F_u = 2A_r f_y = \frac{\pi d^2}{2} \cdot f_y \quad (9)$$

Given that $R = S$, the equilibrium equation can be expressed as Equation (10).

$$2f_y = 8\left(\frac{l_v + l_h}{d}\right)\tau_u + 0.74\sqrt{f_c \cdot f_y} \quad (10)$$

5.2. Variable Statistics

The statistical parameters of the relevant variables can be obtained through a statistical analysis of the results of a large number of previous experimental studies. In GB 50010-2010 (2010), the coefficient of variation for concrete is given. The calculation method for the concrete tensile strength for the compressive strength of concrete prisms is given by Equation (11). The equation for calculation of the concrete tensile strength gives the relevant statistical parameters for the concrete [27], as summarised in Table 5.

$$f_t = 0.267f_c^{\frac{2}{3}} \quad (11)$$

Table 5. Statistical parameters of concrete tensile strength.

Concrete Grade	Symbol	C30	C35	C40
Average value (MPa)	μ_{ft}	2.58	3.12	3.63
Coefficient of variation	δ_{ft}	0.172	0.156	0.149

The research is consistent with the current codes, using the tensile strength design value, f_y , of the steel. The coefficient of variation, $\delta = 0.0641$, has been previously determined [15]. Based on a 95% guarantee rate, the average value of the conditional yield strength, μ_{f_y} , is expressed as Equation (12).

$$\mu_{f_y} = f_y / (1 - 1.645\delta_{f_y}) \quad (12)$$

The rebar specification is HRB400, and the corresponding design value of the tensile strength is 360 MPa; the average yield strength is 402 MPa according to Equation (12). In component geometry, the relevant parameters are obtained according to the statistical results [15], as summarised in Table 6.

Table 6. Statistical parameters for the geometric dimensions of structural members.

Geometric Size	Symbol	Anchor Length l_a^0/l_a^d	Cover Layer c^0/c^d	Rebar Diameter d^0/d^d	Relative Position S_{sv}^0/S_{sv}^d
Average value	μ	1.025	0.9	1	1
Coefficient of variation	δ	0.077	0.30	0.018	0.06

Note: the superscript “0” indicates the measured value, and the superscript “d” indicates the design value.

The accuracy of the calculation model is defined as $\Omega_p = \tau_\mu^t / \tau_\mu^c$, i.e., the ratio of the measured values to the calculated values of the regression statistics; the relevant accuracy parameters are obtained. The average measured values for the rebar are $\mu = 1.058$, $\sigma = 0.122$, and $\delta = 0.115$.

5.3. Target Reliability Indicator

To utilise the strength of the tensile reinforcement fully, a sufficient anchoring length is required to ensure that no bond failure occurs before the rebar yields. Therefore, the conditions at the anchor limit state are that the stress at the free end of the rebar reaches the maximum value (i.e., $\sigma_s = \eta f_y$), and the bond between the rebar and the concrete reaches the maximum value (i.e., $\tau = \tau_u$). This is used as a starting point for determining the reliability of the anchoring performance, and the probability is given by Equation (13).

$$p_{fa} = P(\sigma_s \geq \eta f_y, \tau \geq \tau_u) = P(\sigma_s \geq \eta f_y) \cdot P(\tau \geq \tau_u | \sigma_s \geq \eta f_y) \quad (13)$$

In GB 50068-2001, when structural members experience ductile failure and brittle failure under the second-level safety condition, the design reliability indicators are taken as $\beta = 3.2$ and $\beta = 3.7$, respectively. To ensure that the reliability index of the anchorage performance is higher than the bearing capacity reliability of other component sections, the total reliability index of the anchoring performance design and the corresponding failure probability calculation value are expressed as Equation (14).

$$\beta_a = 3.95, p_{fa} = 4.0 \times 10^{-5} \quad (14)$$

For rebar, the force is designed based on the strength, so when the “free end stress of the rebar reaches the maximum value (i.e., $\sigma_s = \eta f_y$)”, the allowable probability and reliability indicators are based on the standard values, as expressed in Equation (15).

$$\beta = 3.2, p_f = P(\sigma_s = \eta f_y) = 6.87 \times 10^{-5} \quad (15)$$

From Equation (13):

$$p_{f0} = P(\tau = \tau_u | \sigma_s = \eta f_y) = p_{fa} / p_f \quad (16)$$

From Equations (14)–(16), the allowable probability and reliability indicators are expressed in Equation (17).

$$p_{f0} = 5.82 \times 10^{-2}, \beta_{01} = 1.57 \quad (17)$$

According to Schedule 2 in reference [28], the reliability index corresponding to P_{f0} is $\beta_{01} = 1.57$, which is the basis for determining the design value of the anchor length in the anchoring strength problem [29].

In summary, in the analysis of the anchoring problem, the reliability of the anchor design itself is considered to be $\beta = 3.20$, and the anchoring reliability is higher than the reliability of the section design. Relevant experiments [15] have shown that rebar with hooks and bends do not substantially fail to anchor until yielding, and thus additional reliability indices are not considered in this anchoring design.

5.4. Reliability Analysis of the Anchor Length

The approximation method is used to analyze the reliability of the limit state of the bearing capacity. S and R are regarded as two comprehensive basic variables obeying a normal distribution.

5.4.1. Characteristic Parameter for the Effect S

The effect S can be expressed as Equation (18), which is converted from Equation (9).

$$S = 2f_y \quad (18)$$

The average value of S is $\mu_s = 804$ MPa, with a coefficient of variation of $\delta_s = 0.0641$.

5.4.2. Characteristic Parameter of the Resistance (R)

The resistance, R , can be obtained from Equations (8) and (9).

$$R = \Omega_p \cdot R_p = \Omega_p \cdot \left[8 \left(\frac{l_v + l_h}{d} \right) \tau_u + 0.74 \sqrt{f_c \cdot f_y} \right] \quad (19)$$

Based on the situation in this study, Equation (19) can be written as follows:

$$R_p = R(f_t, l_v/d, l_h/d, c/d, f_c, f_y) \quad (20)$$

The statistical parameter of a random variable function can be obtained from the known statistical parameters of the random variable, as expressed in Equations (21)–(23).

$$\mu_{R_p} = R(\mu_{f_t}, \mu_{l_v}, \mu_{l_h}, \mu_{c/d}, \mu_{f_c}, \mu_{f_y}) \quad (21)$$

$$\sigma_{R_p}^2 = \sum_{i=1}^n \left(\frac{\partial R_p}{\partial X_i} \right)_{\mu}^2 \cdot \sigma_{x_i}^2 \quad (22)$$

$$\delta_{R_p} = \frac{\sigma_{R_p}}{\mu_{R_p}} \quad (23)$$

According to the equation for the anchor bond strength, the resistance, R , is expressed as Equation (24).

$$R = 8\Omega_p \cdot \left[\left(\frac{l_v^t + l_h^t}{d^t} \right) \cdot \left(0.82 + 0.9 \frac{d^t}{l_v^t} \right) \left(1.6 + 0.7 \frac{c^t}{d^t} + 12.5 \frac{d^t}{l_v^t} \sqrt{\frac{l_h^t}{l_v^t}} \right) f_t + 0.0925 \sqrt{f_c^t f_y^t} \right] \quad (24)$$

The investigation of the connection reliability is mainly applied to prefabricated shear wall structure systems in this study, and thus, the size of l_h is limited to within a certain range. For the

following situations, the shear wall width is 200 mm, rebar specification is HRB400, and concrete grade is C30; then, $l_h/d = 8$. The statistical parameter of R is thus expressed as Equation (25).

$$\mu_R = 8.464 \cdot \left\{ \left[16.636 + 254.162 \left(\frac{d}{l_v} \right)^{\frac{3}{2}} + 1.875 \frac{l_v}{d} + 28.653 \left(\frac{d}{l_v} \right)^{\frac{1}{2}} + 15.664 \frac{d}{l_v} + 239.308 \left(\frac{d}{l_v} \right)^2 \right] \cdot \mu_{f_t} + \mu_T \right\} \quad (25)$$

5.4.3. Anchor Length

Both the random variables S and R obey lognormal distributions, and a reliable index expression could be given by Equation (26).

$$\beta_0 = \frac{\ln \mu_R - \ln \mu_S}{\sqrt{\delta_R^2 + \delta_S^2}} \quad (26)$$

The calculation equation for the anchor length could be expressed as Equation (27).

$$\ln \mu_R - \ln \mu_S - \beta_0 \sqrt{\delta_R^2 + \delta_S^2} = 0 \quad (27)$$

The relevant statistical parameters for the concrete tensile strength in Tables 4 and 5 are substituted into Equation (27), the equation with unknown factor l_v/d is solved, and the approximate value of the anchor length can be obtained. Considering the concrete grade, the vertical anchor length is given in Table 7. The minimum requirement for the vertical anchoring length of the ring rebar is thus defined.

Table 7. Anchorage lengths of the ring joint.

Content	Symbol	Analysis Results		
Concrete grade	C	C30	C35	C40
Straight anchor section	l_v	$24d$	$19d$	$16d$

6. Design Suggestions

As described in the present study, the vertical length of the rebar plays a critical role in the anchoring performance. It can be summarised as $0.6l_a$ based on the results in Table 7; the curves are shown in Figure 16. In addition, the width of the ring rebar should satisfy $0.4l_a$; the bearing capacity increases and the effect gradually decreases as the size increases.

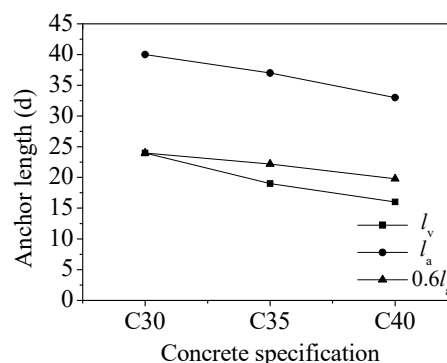


Figure 16. Anchor length curves.

The proposed structural design could ensure the connection performs at its best. The horizontal rebar should be consistent with the ring rebar, and at least two rows of horizontal rebars should be arranged at the corner of the closed area. The ring units should be adjacent to each other within a distance of 25 mm to ensure effective load transmission. The concrete grade should be based on the structural design, and the grade in the connection area should be one level higher than the components

to ensure the stiffness requirements are met. All of these recommendations ensure the mechanical properties of the connection are optimal and promote the application of the ring joint.

7. Conclusions

In this study, experimental and numerical analysis were carried out to analyze the bearing capacity and mechanical mechanism. Then, anchor length was determined based on reliability analysis under various conditions. The conclusions are as follow.

Rebar fracture occurred, and a large number of “V”-shaped cracks were observed on the test pieces. Importantly, the horizontal rebar remained in the flexible stage after yielding of the ring rebar, which was an ideal destruction pattern. The results indicated the joint had a better bearing capacity reserve and ductility. Numerical analysis not only reflected the mechanical mechanism of the internal rebars, but could also be used for further research. A bearing capacity model was proposed considering the bond and dowel actions simultaneously, and it could predict the bearing capacity well. The dowel action of the horizontal rebars could improve the bearing capacity and avoid the risk of the ring rebar being pulled out under reasonable design. The anchor length, l_v , was determined based on the reliability analysis, and other structural measures has been proposed, which could guarantee the mechanical properties and reliability of the ring joint.

Author Contributions: All authors participated equally in the design and implementation processes of this manuscript. They all participated in drafting the article or revising it critically for important intellectual content. Final approval of the version to be submitted was given by all authors. Conceptualization, X.Z., F.F. and A.J.; methodology, J.Z. and H.Q.; software, J.Z.; validation, J.Z., X.Z.; formal analysis, J.Z. and X.Z.; investigation, all of the authors; resources, X.Z. and F.F.; data curation, J.Z. and X.Z.; writing—original draft preparation, J.Z. and X.Z.; writing—review and editing, all of the authors; visualization, J.Z.; supervision, F.F. and A.J.; project administration, X.Z.; funding acquisition, X.Z. All authors read and approved the final manuscript.

Funding: This research was funded by the Special Project of National Key Research and Development Plan, grant number No. 2017YFC0703804.

Acknowledgments: The authors gratefully acknowledge the financial support by the Special Project of National Key Research and Development Plan. The help of the China Construction Seventh Engineering Division Corp. Ltd. is sincerely appreciated.

Conflicts of Interest: The authors declare no conflict of interest.

Notation

A_r	cross-sectional area of the up-ring rebar
c	thickness of the concrete cover
d	diameter of the rebar
d_h	diameter of the horizontal rebar
f_c	compressive strength of concrete
f_t	design value of the concrete axial tensile strength
f_y	yield strength of the rebar
f_{y-R}	load at yielding of the ring rebar
f_{y-HR}	load at yielding of the ring rebar when the strength is increased
l_h	anchorage length of the rear anchor section of rebar
l_v	anchorage length of the straight anchor section of rebar
P	bearing capacity of the ring joint
R_p	calculated resistance
$R(\bullet)$	function of each random variable
X_i	random variable in function $R(\bullet)$
X	material coefficient
τ_u	reduced ultimate anchoring strength
Ω_p	accuracy coefficient of the calculation equation

References

1. Liu, H.T.; Han, Q.; Bai, Y.L.; Xu, C.S. Connection performance of restrained deformed grouted sleeve splice. *Adv. Struct. Eng.* **2018**, *21*, 488–499. [\[CrossRef\]](#)
2. Soudki, K.A.; Rizkalla, S.H.; Leblanc, B. Horizontal connections for precast concrete shear wall subjected to cyclic deformations part 1: Mild steel connections. *PCI J.* **1995**, *40*, 78–96.
3. Soudki, K.A.; Rizkalla, S.H.; Daikiw, R.W. Horizontal connections for precast concrete shear walls subjected to cyclic deformations part 2: Prestressed connections. *PCI J.* **1995**, *40*, 82–96. [\[CrossRef\]](#)
4. Soudki, K.A.; West, J.S.; Rizkalla, S.H.; Blackett, B. Horizontal connections for precast concrete shear wall panels under cyclic shear loading. *PCI J.* **1996**, *41*, 64–80. [\[CrossRef\]](#)
5. Einea, A.; Yamane, T.; Tadros, M.K. Grout-filled pipe splices for precast concrete construction. *PCI J.* **1995**, *98*, 82–93. [\[CrossRef\]](#)
6. Kim, Y.M. A Study of Pipe Splice Sleeves for Use in Precast Beam-Column Connections. Master's Thesis, University of Texas, Austin, TX, USA, 2000.
7. Haber, Z.B.; Saiidi, M.S.; Sanders, D.H. Seismic performance of precast columns with mechanically spliced column-footing connections. *ACI Struct. J.* **2014**, *111*, 639–650. [\[CrossRef\]](#)
8. Popa, V.; Papurcu, A.; Cotofana, D.; Pascu, R. Experimental testing on emulative connections for precast columns using grouted corrugated steel sleeves. *Bull. Earthq. Eng.* **2015**, *13*, 2429–2447. [\[CrossRef\]](#)
9. Qian, J.R.; Yang, X.K.; Qin, H. Test on seismic behavior of pre-cast shear walls with various methods of vertical reinforcement splicing. *J. Build. Struct.* **2011**, *32*, 51–59. (In Chinese)
10. Zhu, Z.F.; Guo, Z.X. Seismic test and analysis of joints of new precast concrete shear wall structures. *China Civ. Eng. J.* **2012**, *45*, 69–76. (In Chinese)
11. Hosseini, S.J.A.; Rahman, A.; Baharuddin, A. Analysis of spiral reinforcement in grouted pipe splice connectors. *Gradevinar* **2013**, *65*, 537–546.
12. Zheng, Y.F.; Guo, Z.X.; Liu, J.B.; Chen, X.N. Performance and confining mechanism of grouted deformed pipe splice under tensile load. *Adv. Struct. Eng.* **2016**, *19*, 86–103. [\[CrossRef\]](#)
13. Zheng, Y.F.; Guo, Z.X.; Guan, D.Z.; Zhang, X. Parametric study on a novel grouted rolling pipe splice for precast concrete construction. *Constr. Build. Mater.* **2018**, *166*, 452–463. [\[CrossRef\]](#)
14. Jiang, H.B.; Zhang, H.S.; Liu, W.Q.; Yan, H.Y. Experimental study on plug-in filling hole for steel bar lapping of precast concrete structure. *J. Harbin Inst. Technol.* **2011**, *43*, 18–23. (In Chinese)
15. Shao, Z.M.; Shen, W.D.; Xu, Y.L. Anchorage reliability and anchoring design of reinforced concrete. *J. Build. Struct.* **1987**, *8*, 36–49. (In Chinese)
16. Liu, Q.W.; Wu, T.; Cheng, R. Experiment research and reliability analysis on grouted-filled lap splice. *Bull. Chin. Ceram. Soc.* **2018**, *37*, 1324–1331. (In Chinese)
17. Lu, X.L.; Wang, L.; Wang, D.; Jiang, H.J. An innovative joint connecting beam for precast concrete shear wall structures. *Struct. Concr.* **2016**, *17*, 972–986. [\[CrossRef\]](#)
18. Jiao, A.L.; Zhang, P.; Li, Y.H.; Zhi, X.D. Tests on seismic behavior of pre-cast shear walls with annular closed reinforcements. *J. Build. Struct.* **2015**, *36*, 103–109. (In Chinese)
19. Gao, Y.F.; Jiao, A.L.; Zhang, Z.S.; Liu, J.; Zhi, X.D. Tests on out-of-plane bending of precast shear walls with annular closed reinforcements. *Build. Struct.* **2016**, *46*, 439–442. (In Chinese)
20. Amadio, C.; Bedon, C.; Fasan, M.; Pecce, M.R. Refined numerical modelling for the structural assessment of steel-concrete composite beam-to-column joints under seismic loads. *Eng. Struct.* **2017**, *138*, 394–409.
21. Li, J.; Wang, J.Y. Elastoplastic damage constitutive model for concrete based on damage energy release rates, part I: Basic formulations. *China Civ. Eng. J.* **2005**, *38*, 14–20. (In Chinese)
22. Zhi, X.D.; Fan, F.; Shen, S.Z. Application of material damage cumulation in reticulated shells under severe earthquakes. *J. Harbin Inst. Technol.* **2008**, *40*, 169–173. (In Chinese)
23. Nakaki, S.D. An overview of the PRESS five-story precast test building. *PCI J.* **1999**, *44*, 26–39. [\[CrossRef\]](#)
24. Kulkarni, S.A.; Li, B.; Yip, W.K. Finite element analysis of precast hybrid-steel concrete connections under cyclic loading. *J. Constr. Steel Res.* **2008**, *64*, 190–201. [\[CrossRef\]](#)
25. Li, P.F.; An, X.H.; He, S.Q.; Chen, C. Three-dimensional bond model considering the coupled damage effect for dowel action. *Mag. Concr. Res.* **2017**, *69*, 728–744. [\[CrossRef\]](#)
26. Rasmussen, B.H. The carrying capacity of transversely loaded bolts and dowels embedded in concrete. *Bygn. Meddelser* **1963**, *34*, 39–55.

27. Teng, Z.M.; Luo, F.T.; Shi, L.Q. *Reinforced Concrete Basic Member*; Tsinghua University Press: Beijing, China, 1987. (In Chinese)
28. Zhao, G.F. *Advanced Structural Science of Reinforced Concrete*; China machine Press: Beijing, China, 1999. (In Chinese)
29. Mou, X.G. Experimental Study and Numerical Simulation of Bond Behavior of High-Strength Prestressed Reinforcement. Ph.D. Thesis, Dalian University of Technology, Dalian, China, 2006. (In Chinese).



© 2019 by the authors. Licensee MDPI, Basel, Switzerland. This article is an open access article distributed under the terms and conditions of the Creative Commons Attribution (CC BY) license (<http://creativecommons.org/licenses/by/4.0/>).